Photocatalytic transformation of flufenacet over TiO2 aqueous suspensions: Identification of intermediates and the mechanism involved

Photocatalytic transformation of flufenacet over TiO_2 aqueous suspensions: Identification of intermediates and the mechanism involved

V.A. Sakkas[a], P. Calza[b,c], A.D. Vlachou[a], C. Medana[b], C. Minero[b,c], T. Albanis[a]

[a] *Department of Chemistry, University of Ioannina, Ioannina 45110, Greece*

[b] *Department of Analytical Chemistry, University of Torino, via P. Giuria 5, 10125 Torino, Italy*

[c] *NIS Centre Excellence, , via P. Giuria 7, 10125 Torino, Italy*

** Corresponding author: Tel.: +39 0116707626; fax: +39 0116707615.*

E-mail address: paola.calza@unito.it (P. Calza)

Abstract

In order to exploit the efficiency of titania suspensions in photocatalysis for the degradation of the herbicide flufenacet, chemometric optimization tools were employed, such as response surface methodology and experimental design. The aqueous samples were irradiated under a variety of experimental conditions with different amounts of catalyst (TiO_2), electron acceptor (H_2O_2) as well as pH. Results indicated that the degradation efficiency of the herbicide in the experimental domain investigated was mainly affected by the concentration of H_2O_2, followed by TiO_2, pH, as well as their interaction effects.

Additionally, the phototransformation products formed during the photocatalytic process were investigated and characterized by means of HPLC/HRMS. The photocatalysed transformation of flufenacet proceeds through the formation of thirty-two (32) products, involving reactions of mono- and di-hydroxylation, dealkylation, detachment of the thiadiazole ring, defluorination on the benzene ring followed by the detachment of the latter ring. The thiadiazole ring appears to be involved in the process to a lesser extent and only as a secondary path. The measurement of acute toxicity, evaluated using the *Vibrio fischeri* bacteria test, showed that the transformation of flufenacet proceeds through the formation of compounds more toxic than the parent molecule. Although the identified intermediates were easily degraded and within two hours of irradiation were completely disappeared, mineralization was much slower and complete formation of CO_2 and inorganic constituents was only achieved after 24 h of irradiation.

Keywords: Photocatalysis, TiO_2, experimental design, mineralization, toxicity, flufenacet

1. Introduction

Addition of any natural or artificial foreign matter from various sources, such as industrial effluents, agricultural runoff and chemical spills, contaminates the water [1]. These effluents include several non-biodegradable, toxic organic substances, like herbicides, dyes, phenols, PhACs, PCPs etc. These substances are toxic, stable to natural decomposition and are persistent to the environment [2].

The acetamide herbicides, including flufenacet, are an important class of herbicides in the United States and in Europe [3]. Flufenacet (N-(4-fluorophenyl)-N-(1-methylethyl)-2-[[5-(trifluoromethyl) -1,3,4-thiadiazol-2- yl]oxy]acetamide) molecular structure is shown later in Scheme 2. It is used as pre-emergence or with shallow soil incorporation to control annual grasses and some broadleaf weeds in a variety of crops. It displays relatively high solubility in water (56 mg/L) and is particularly stable against hydrolysis (pH 5: 14835 days, pH 7: 1547 days, pH 9: 654 days) [4] and photolysis [5]. Its chemical stability along with its mobility enables this herbicide to cause contamination of the ground water via leaching through soil as well as surface water supplies via dissolved run-off and/or erosion [6]. Levels of 0.07 μg/L of flufenacet have been reported in Lamspringe, Germany, and were dependent on the amount applied, type, time, duration and number of application(s), soil management, site characteristics (soil type, crop) as well as climatic conditions [7].

Treatments of laboratory animals with flufenacet resulted in depression of total and free-serum thyroxin levels and in transient and dose related changes in circulating levels of tri-iodothyronine and thyrotropin. Liver changes, which included tissue mass, hypertrophy of hepatocytes, increased cytochrome P450 content and proliferation of the endoplasmic reticulum, were suggestive of induction of mixed function oxidase activity with the apparent purpose to facilitate the metabolism and excretion of the chemical [8].

Due to its properties, flufenacet is of special interest since it presents potential for threatening the environment and human health. Indeed, exposure to agricultural chemicals has been linked to reduced stamina and cognitive abilities in children [9] and increased incidence of human birth malformations [10].

Hence, there is a need to develop effective purification methods for eliminating it from water. Among the different AOPs that have been proposed for the degradation of organic micro-pollutants, TiO_2-mediated photocatalysis has shown to be an advantageous technology as it can be carried out under ambient conditions and may lead to complete mineralization of pollutants to CO_2, water and mineral acids. TiO_2 is by far the most widely used semiconducting material, because of its chemical inertness, photostability, low cost and non-toxicity. The degradation of pollutants by means of TiO_2 is well documented in the literature [11-12]. Photocatalytic processes mated with chemometric experimental design play a crucial role for their ability to understand the statistically significant variables affecting the process and reaching the optimum of the catalytic reactions.

The main objectives of this research were to assess the degradation of the pollutant through combined evaluation of different aspects: (i) the optimization of the degradation procedure by means of a central composite design, studying the simultaneous effect of TiO_2, pH and H_2O_2 concentration on the degradation efficiency, (ii) the identification of intermediates, in order to establish the reaction pathways, (iii) the evolution of mineralization and (iv) the assessment of the toxicity along the photocatalytic reactions by means of luminescence bioassays using *Vibrio fischeri*.

The present manuscript describes for the first time the pathways for the formation of different transformation products of flufenacet, the elucidation of mechanistic details of the conversion, the mineralization evaluation, as well as the toxicity assessment.

2. Experimental

2.1. Material and reagents

Flufenacet (purity higher than 99%) was supplied by Riedel-de-Häen (Seelze-Hannover, Germany). Solvents used: acetonitrile (Aldrich) and methanol (BDH) were filtered through a 0.45 μm filter before use. Analytically pure grade hydrogen peroxide (30%) used in the experiments was from Merck (Darmstadt, Germany). Experiments were carried out using TiO_2 Degussa P25 as the photocatalyst. In order to avoid possible interference from ions adsorbed on the photocatalyst, the TiO_2 powder was irradiated and washed with distilled water.

2.2. Irradiation procedures

Irradiation experiments were performed on stirred aqueous solutions contained in a cylindrical quartz glass UV-reactor. Degradations were carried out on 50 mL of aqueous flufenacet solutions with varying pH, initial concentrations of TiO_2 and H_2O_2 according to the experimental design (Table 1). Before irradiation, the suspensions were allowed to stay in the dark for 60 min under stirring, to reach adsorption equilibrium on the semiconductor surface. UV-reactor containing the solution was introduced into a Suntest CPS+ apparatus from Heraeus (Hanau, Germany) equipped with a xenon arc lamp (1500W) and special glass filters restricting the transmission of wavelengths below 290 nm. Chamber and black panel temperature were regulated by pressurized air cooling circuit and monitored using thermocouples supplied by the manufacturer. The temperature of samples did not exceed 20°C using tap water cooling circuit for the UV-reactor.

Irradiation experiments on intermediates have been performed in air saturated conditions using a Blacklit Philips TLK/05 lamp (40 W/m^2) with the maxima emission at 360 nm. Irradiation

experiments were carried out in Pyrex glass cells containing 5 mL of flufenacet (15 mg/L) and TiO_2 (200 mg/L). The temperature reached during the irradiation was 38 ± 2°C.

Before analysis with the appropriate technique, aliquots taken at specific time intervals from UV-reactor and the entire content of the cells was filtered through 0.45 μm PVDF Millipore membrane filters to remove titania particles.

2.3. Analytical procedures

2.3.1. Liquid- chromatography-MS

The chromatographic separations followed by a MS analyzer were run on a C18 column Phenomenex Luna, 150 × 2.0 mm, thermostated at 30°C using an Ultimate 3000 HPLC instrument (Dionex, Milan, Italy). Injection volume was 20 μL and flow rate 200 μL/min. Gradient mobile phase composition was adopted: 5/95 to 100/0 in 35 min. acetonitrile/formic acid 0.05% in water. A LTQ Orbitrap mass spectrometer (Thermo Scientific, Bremen, Germany) equipped with an atmospheric pressure interface and an ESI ion source was used as detector. The LC column effluent was delivered into the ion source using nitrogen as sheath and auxiliary gas. The source voltage was set at the 4.5 kV value. The heated capillary value was maintained at 265°C. The acquisition method used was previously optimized in the tuning sections for the parent compound (capillary, magnetic lenses and collimating octapoles voltages) in order to achieve the maximum of sensitivity. The tuning parameters adopted for ESI source have been the following: capillary voltage 7.00 V, tube lens 55 V; for ions optics, multipole 00 offset -1.50 V, lens 0 voltage - 5.50 V, multipole 0 offset - 4.75 V, lens 1 voltage -36.00 V, gate lens voltage - 80.00 V, multipole 1 offset -19.50 V, front lens voltage - 5. 50 V. Mass accuracy of recorded ions (vs calculated) was ± 5 millimass units (mmu) (without internal calibration).

2.3.2. Liquid- chromatography-UV

The chromatographic analysis for phenol derivatives were followed by a UV-Vis detector (Merck Hitachi L-4200) and were accomplished by an HPLC using a Rheodyne injector, a RP C18 column (Lichrochart, Merck, 12.5 cm × 0.4 cm, 5 μm packing) and a gradient made by two high pressure pumps (Merck Hitachi L-6200 and L-6000 pumps). Gradient mobile phase composition was adopted: 20/80 to 50/50 in 10 min. methanol/phosphate buffer 0.01 M at pH 2.8.

2.3.3. Ion chromatography

A Dionex instrument was employed equipped with a conductometer detector. The determination of ammonium ions was performed by adopting a column CS12A and 25 mM metansulphonic acid as eluant, at a flow rate of 1 mL/min. In such conditions, the retention time of ammonium was 4.7 min. The anions were analysed by using an AS9HC anionic column and a mixture of $NaHCO_3$ 12 mM and K_2CO_3 5mM at a flow rate of 1 mL/min. In these experimental conditions the retention times of fluoride, nitrite, nitrate and sulphate were 4.0,7.0, 8.3, 9.6 and 22.6 min, respectively.

2.3.4. Total organic carbon analyzer

Total organic carbon (TOC) was measured on filtered suspensions using a Shimadzu TOC-5000 analyzer (catalytic oxidation on Pt at 680°C). The calibration was performed using standards of potassium phthalate.

2.3.5. Toxicity measurements

Acute toxicity of an unirradiated flufenacet solution and of aqueous samples collected at different irradiation times was examined by Microtox Model 500 Toxicity Analyzer. The analysis is based on the measurement of the ability of the sample to inhibit the natural bioluminescence of the marine bacterium *Vibrio fischeri* when challenged with toxic compounds. Freeze-dried bacteria were activated and samples were tested in a medium containing 2% sodium chloride, in five dilutions. After 15 min of incubation at 15^{o}C light emission was recorded and compared with a toxic-free

control. The percentage of inhibition was calculated following the established protocol using the Microtox calculation software.

2.4. Response surface methodology and experimental design

Response surface methodology is a collection of statistical and mathematical techniques useful for developing, improving and optimizing processes [13]. Besides the evaluation of relations existing between a group of controlled experimental factors and the observed results (of one or more selected criteria) RSM can derive a model that represents the whole process. Therefore, the application of statistical experimental design techniques in the development of the photocatalytic process can result in improved degradation efficiencies, reduced process variability combined with the requirement of less resources (time, reagents and experimental work) [14-15].

At first, two-level fractional factorial design (resolution III) with five factors was used in order to eliminate unimportant factors before investing time and money in a more elaborate experiment. Five factors: pH, light intensity, flufenacet concentration, TiO_2 and H_2O_2 concentrations were chosen, according to our previous experience dealing on the photocatalytic processes of micropollutants [16-18]. From the analysis of data (data not shown) pH, TiO_2 and H_2O_2 have significant impact ($p < 0.05$) on flufenacet degradation. The curvature was also significant, indicating that a higher order model or response surface study is needed in order to uncover the behavior of the significant factors. Central composite design (CCD), which is a widely used form of RSM, was employed for the investigation the simultaneous effect of TiO_2, H_2O_2 and pH with respect to the photocatalytic process as well as to evaluate the interactions between the three variables. For this design, 17 experiments were performed, at which the three variables (TiO_2, H_2O_2 and pH) were codified in five levels with three central points (Table 1). Experimental data based on the degradation percentage (%) of flufenacet after 30min of the photocatalytic treatment procedure were analyzed using the STATISTICA® software. The profile for predicted values and desirability option was used for the optimization of the process.

3. Results and discussion

3.1. Flufenacet stability and photolysis

Preliminary experiments were carried out, before the development of the experimental design, to evaluate the extent of adsorption, hydrolysis and photolysis processes on the transformation. Results obtained showed that the experiments occurred in a pure photocatalytic regime where hydrolysis and photochemical processes can be neglected. Results obtained by the adsorption in the dark showed a slight decrease of flufenacet concentration (about 10%) for a time period of 2h, which indicates that it was only negligibly adsorbed on the TiO_2 surface. Hydrolysis as well as direct photolysis (2h) showed no transformation of the pollutant. This proves that the above abiotic processes were scarcely responsible for the observed fast transformations during the experiments.

3.2. Kinetics of disappearance

Several experimental results indicated that the destruction rates of photocatalytic oxidation of various organic contaminants over illuminated TiO_2 followed a saturative trend with increasing the substrate concentration similar to a Langmuir–Hinshelwood behavior that was strongly criticized [19-20].

Taking into consideration the recent point of discussion with regards to kinetics interpretation in photocatalytic reactions, [21] to reduce experiments and related times for the development of multivariate approach, the efficiency of the photocatalytic procedure was evaluated as the degradation percentage after 30 min of light irradiation (Table 1, fourth column). This time period was chosen because distinguishable amounts of flufenacet was obtained that allowed better comparison of the results.

3.2.1. Response surface methodology

TiO_2 (x_1), pH (x_2) and H_2O_2 (x_3) were the input variables in order to get the degradation efficiency% (response) of flufenacet. The complete design matrix (experimental conditions), range, levels of factors and the obtained results, are summarized in Table 1. The fourth column in Table 1 shows the experimental values (in terms of Flufenacet degradation yield after 30 min of irradiation) obtained for the response factor (Y) and the fifth column the calculated values by way of the modeling procedure. Experiments were undertaken in random order to provide protection against the effects of lurking variables.

The sufficiency of the model was evaluated through analysis of variance (ANOVA). Moreover, Lack of Fit (LOF, i.e., the variation of the data around the fitted model) was also checked and was shown to be not significant relative to the pure error, indicating good response to the model. The model regression coefficient (R^2) of 0.9722 is in reasonable agreement with the experimental results, indicating that 97.22% of the variability can be revealed by the model 2.78% only residual variability remains. As well, the adjusted determination coefficient (adjusted R^2 = 0.93042) is also very high to advocate for a high significance of the model. Both values ensured a satisfactory adjustment of the polynomial model to the experimental data.

Data analysis using the STATISTICA software at 95% of confidence level permitted to obtain a semi-empirical expression (Eq. 1) in terms of significant coded factors

$$Y= 88,72(\pm0,11) + 6,77(\pm0,09)x_1 - 6,43(\pm0,11)x_1^2 - 6,76(\pm0,09)x_2 + 4,58(\pm0,11)x_2^2 – 10,61(\pm0,09)x_3 + 1,69(\pm0,11)x_3^2 + 3,92\ (\pm0,12)x_1x_2 – 6,35(\pm0,12)x_2x_3 \quad (1)$$

where $x_1=[TiO_2]$, x_2= pH, $x_3=[H_2O_2]$. This mathematical expression represents the response factor that is given by the percentage of flufenacet degradation obtained from the decrease of its concentration after 30min of photocatalytic reaction. The coefficients of the quadratic model in the equation were calculated by least-square multiple regression analysis. The importance of each variable depends on its signs and values as well as on the relative error (absolute value) associated

to each value, which is indicated in parenthesis of Eq. (1). Positive coefficients indicate that degradation is favoured in the presence of high concentrations of the respective variable within the range studied, while negative coefficients indicate that the reaction is favoured in the presence of low concentrations. Positive quadratic coefficients of x_1x_2 variables indicate a synergistic effect, while negative coefficients of x_2x_3, an antagonistic effect between the variables.

For visualization of the calculated factor effects, the Pareto graph is presented in Fig. 1. In this graph, the ANOVA effect estimates are sorted from the largest absolute value to the smallest. The magnitude of each effect is represented by a column, and often, a line going across the columns indicates how large an effect has to be (i.e., how long a column must be) to be statistically significant. All the standardized effects which overpass the significance line (vertical line) exert a statistically significant influence on the degradation (%) of flufenacet. As it can be seen, the most important parameter of the overall treatment procedure was H_2O_2 concentration, followed by TiO_2 and pH. Results have shown that the degradation of the herbicide was, also, significantly affected by two variable interactions, between TiO_2 and pH, as well as pH and H_2O_2.

The overall interaction effects are displayed in Fig. 2; a 3-D representation of the polynomial (Eq. (1)) obtained from the experimental data.

As shown in Fig. 2a (TiO_2, pH) the degradation rate increases proportionally to TiO_2 concentration confirming the positive influence of the increased number of TiO_2 active sites on the process kinetics. At higher catalyst loading, however, a slight decrease of the efficiency was observed, irrespective of the initial pH. Whether in static, slurry or dynamic flow reactors, it has been observed that above a certain concentration, the reaction rate levels off and becomes independent of the catalyst concentration because of light scattering and screening effects. Moreover the tendency towards agglomeration (particle-particle interaction), also, increases at high solids concentration, resulting in a reduction in catalyst's surface area available for light absorption and hence a drop in degradation rate. Although the number of active sites in solution will increase with catalyst loading,

a point appears to be reached where light penetration is compromised because of excessive particle concentration and turbidity. Similar observations have been also reported in other studies on various organic substances [12, 22-23].

The interpretation of pH effect on the photocatalytic reaction is a difficult task because of its multiple role, such as electrostatic interactions between the titania surface, solvent molecules, substrate and charged radicals formed during the process. For pH values higher than the point of zero charge (PZC, 6.8 [24]) of titania, the surface becomes negatively charged and it is the opposite for pH < PZC.

As shown in Fig. 2a, the efficiency of the photocatalytic degradation of flufenacet depends on the initial pH of the aqueous solution. Lower degradation rates were observed at pH values close to PZC. This phenomenon can be explained by the tendency of titania particles to agglomerate causing a reduction on the photocatalytic yield. As it has been reported at pH equal to PZC the particles aggregate and ensembles are larger, causing a decrease in the surface active sites and an increase of scattering affecting the degradation rates [19, 25-27]. The TiO_2 suspension is colloidally stable at both acid and basic pH and therefore higher degradation % of flufenacet is observed.

The effect of pH on the photocatalytic reaction may also be explained by the surface charge of titania and its relation to the physicochemical properties of the parent molecule. Despite of being a neutral molecule, flufenacet could be repulsed by the negative charged titania particles above pH 6.8 because of the imbalance of charge distribution and the existence of the electronegative atoms [27]. However, at moderate to high amounts of TiO_2 at basic pH degradation rates are increasing-attributed to the increase in the number of OH groups at the titania surface, since OH· can be formed by trapping photoproduced holes.

Considering the interaction between pH and H_2O_2 (Fig. 2b) at fixed TiO_2 concentration, one can see that when low amounts of H_2O_2 are introduced, rate enhancement is likely due to the increased

generation of $HO^{\bullet}$. Moreover, H_2O_2 reacts with the electrons which are emitted from the valence band of the catalyst to generate $HO^{\bullet}$ and OH^- (instead of generating a weaker $^{\bullet}O_2^-$ radical). If these reactive species, such as oxygen and H_2O_2, are not present nearby the surface of the TiO_2, the electron-hole pair will recombine and the energy absorbed will be dissipated as heat. Therefore, at low dosage of H_2O_2, H_2O_2 is capable of partly suppress the electron hole pair from recombination [28-29].

However, when H_2O_2 is overdosed, the photodegradation is retarded. The excess H_2O_2 molecules scavenge the valuable $HO^{\bullet}$ that are generated by either the direct photolysis of H_2O_2 or the photooxidation of OH^- by h^+ and generate a much weaker hyperoxyl radical, $HO_2^{\bullet}$. The $HO_2^{\bullet}$ radical can further react with the remaining strong $HO^{\bullet}$ to form ineffective oxygen and water.

$$HO_2^{\bullet} + HO^{\bullet} \rightarrow H_2O + O_2 \quad (2)$$

In addition, the oxidation could be inhibited when the excess H_2O_2 reacts with oxidative h^+ on catalyst surface, where the overall oxidation capabilities of the system are significantly reduced by generating oxygen [30]:

$$H_2O_2 + 2h_{VB}^+ \rightarrow O_2 + 2H^+ \quad (3)$$

Low degradation efficiency at high pH and H_2O_2 values may be attributed to the fact that H_2O_2 becomes unstable and self-decomposition occurs. The self-decomposition that is strongly dependent on pH [31] will rapidly break down the H_2O_2 molecules into water and oxygen and in such a way oxidant characteristics are lost.

The desirability function for degradation of flufenacet was defined by assigning a desirability value of 0.0 for degradation% below 70.92, of 1.0 for values above 99.83 and 0.5 for 85.37. In order to achieve the highest desirability score (desirability 1), software optimized 88.72% degradation of flufenacet with calculating the optimized model factors (pH, TiO_2 and H_2O_2 concentration) and the optimum values of the factors for the maximum degradation % are depicted (Figure 3). These

figures allow seeing at a glance how changes in the level of each variable affect the response (degradation %), and, at the same time, the overall desirability of the responses.

Finally, for validation, duplicate assenting experiments were conducted using the optimized parameters. The results are closely co-related with the data obtained from desirability optimization analysis using central composite design (CCD), indicating that CCD with desirability function could be effectively used to optimize the photocatalytic degradation of the target analyte. A usual requirement for an efficient catalytic reaction is its application, or in other words, the ability of the optimized method to provide accurate and precise results despite variations in equipment and conditions. For this reason the target compound was tested at the optimal conditions found from RSM coupled to desirability function, in natural river water (pH 7.82, conductivity 343 mS/cm, total dissolved solids 193 mg/L, total organic carbon 2.31 mg/L). Results have shown that the response of interest (degradation efficiency) was not significantly influenced by changing the aqueous matrix from distilled to natural river water demonstrating a yield of 83% after 30 min of illumination.

3.3. Flufenacet degradation and identification of the transformation products

Along with flufenacet decomposition ($t_{1/2}$ = 5 min, see later in Figure 7), the formation of 32 intermediate compounds (TPs) occurred. Formation of 28 TPs was detected by HPLC/MS; *m/z* ratios, proposed elemental composition, product ions and retention times are collected in Tables 2 and 3; Table 2 collects all the species involving an initial hydroxylation (showed in Scheme 2), while Table 3 collects all compounds involving N-dealkylation or defluorination. As well, their time evolution curves are shown in Fig. 4 for compounds collected in Scheme 2 and in Fig 5 for phototransformation products shown in Scheme 3. In addition, few phenolic compounds were identified by HPLC/UV through injection of a commercially available standard solution, namely

phenol (labelled **XVI**), catechol (labelled **XVII**) and 4-fluorophenol (labelled **VII**), all plotted in Fig. 4 and 5. These TPs are formed in the initial steps of the phototransformation treatment. Their highest level were observed when more than half of the flufenacet was transformed. Most of these TPs were readily transformed and after 2h of irradiation they were completely abated.

Analyses by HPLC/MS were run in the ESI positive mode, which appears to be more sensitive and suitable for most of the TPs. Flufenacet MS^n spectra showed as key fragmentation pathway the loss of hydroxy-thiadiazole ring with the formation of the product ion at *m/z* 194.0964, whose further fragmentation produced an ion at *m/z* 152.0494 via N-dealkylation (see Scheme S1 in supplementary material and Table 2); these routes have been carefully considered in the structure attribution of unknown compounds. The positive-ion ESI mass spectra of flufenacet transformation products provided a simple means for the determination of the molecular mass. High resolving power was useful to attribute their empirical formula; accurate masses of parent ions were reported with error below 1 mmu, which guarantee the correct assignment of their molecular formula in all cases, while their MS^2 and MS^3 spectra showed several structural-diagnostic ions that allowed to characterize the different TPs and to distinguish the isobaric species. The proposed structures are consistent with the fragmentation profiles of their protonated forms, as shown in Scheme 1 for compounds at *m/z* 380.0692 and in supplementary information for all other intermediate products (see Schemes S2-S8). All these transformation products can be grouped as reported in Scheme 2 and 3 and, taking into account their evolution time, they should be formed through the occurrence of seven concomitant pathways, labelled **A-G**.

The initial pathways **A-D** involved hydroxylation and are shown in Scheme 2. All the described processes occurred without involving the ring(s) cleavage and/or defluorination. Five different peaks at *m/z* 380.0692 (compounds **IA-IE**), attributed to flufenacet mono-hydroxyderivatives, were produced as a consequence of the non specific OH radical attack. These compounds followed diverse fragmentation pattern that, even if cannot allow to univocally attribute a single structure,

however permits to subdivide these compounds into three groups: 1) isomers 380-A and C, whose unusual fragmentation patterns involves fluorine radical loss, should indicate that the hydroxylation took place at the phenyl ring. However, the specific places for OH radical attack in the ring could not be elucidated with the available MS^n information; 2) isomers 380-B and 380-E reasonably hold the OH group on the alkyl chain. Both species showed the product ion at *m/z* 362.0588 formed by loss of a water molecule as MS^2 base peak and, for 380-E, a fragment at *m/z* 138.0712, well fit with the presence of unmodified phenyl ring; 3) isomer 380-D should hold the OH group on the acetanilide moiety, as assessed by the structural-diagnostic ion at *m/z* 180.0820 where both the alkyl chain and the phenyl ring are unmodified. These compounds start different flufenacet transformation routes, namely pathway **A**, when hydroxylation involves the benzene ring, pathways **B** and **D**, when involving the alkyl chain or pathway **C**, if the acetanilide moiety is involved. Pathway **A** proceeds through a second step of hydroxylation (see compound **II**) or could alternatively involve an oxidation with the formation of compound **III-A**. Compound **II**, yielding a *m/z* ratio of 396.0364, is consistent with the flufenacet dihydroxyderivative; it produced as major fragments the ions at *m/z* 184.0358 and 226.0878, so implying that both OH radical attack involved the phenyl ring (see Scheme **S2**).

Three isobaric species at *m/z* 378.0536 are formed. This accurate mass corresponded to the formula $C_{14}H_{12}O_3N_3F_4S$, which is consistent with the oxidation of the alcoholic group into a keto group (compounds **IIIA - IIIC**). MS^2 analysis allowed characterizing two of these compounds (**III-B** and **III-C**) as **I-B** and **I-D** oxidative derivatives as described in Scheme **S3** and Scheme 2. It has to be underlined that the structural information obtained by means of MS^2 analysis was not sufficient to unequivocally predict a structure for isomer **A,** but is consistent with the structure shown in Scheme 2, deriving from I-A transformation.

Three isobaric species at *m/z* 268 characterized by different accurate mass were formed (compounds **VIII**) (for isomer A: 268.0378 and empirical formula $C_8H_9O_2N_3F_3S$, for isomers B and C 268.0102

and empirical formula $C_7H_5O_3N_3F_3S$) and are consistent with the further transformation of compounds **III** by the detachment of fluorophenyl moiety. This hypothesis is corroborated by MS^2 spectra analyses (see Scheme **S4** for structural attribution) and by the contemporaneous formation of 4-fluorophenol. In addition, the formation of a TP at *m/z* 194.0613 (molecular formula $C_{10}H_9O_2NF$, compound **V** in scheme **S5**) occurred. Even if the structural information obtained by means of MS^2 analysis was not sufficient to unequivocally predict a structure for this compound, we tentatively proposed the structure shown in Scheme 2. Pathways **B** and **C** proceeds then through oxidation of the alcoholic group (compound **III-B** and **III-C**) followed by fluorophenyl detachment (compound **VIII-B** and **VIII-C**) or through route D with the formation of compound **VIII-A**.

In competition with pathway ***C.i***, the detachment of thiadiazole ring could occur as described in pathway ***C.ii***. The contemporaneous formation of oxanil acid (OXA-flufenacet, **VI**), a flufenacet degradation product already found in natural water [32], and 5-trifluoromethyl-2-hydroxyl-1,3,4-thiadiazole (**IV**) supports this hypothesis. Successively, the molecule breakage occurs, followed by the oxidation of lateral chains and, again, 4-fluorophenol (**VII**) should be formed.

Flufenacet initial transformation could also be initiated by N-dealkylation, as described in pathway **E** shown in Scheme 3. A calculated mass *m/*z 322.0273 was obtained for the protonated molecule of the intermediate **IX.** The empirical formula $C_{11}H_8O_2N_3F_4S$ and the fragmentation pattern producing two product ions common to flufenacet product ion at $[M+H-C_3H_6]^+$ are well matched with the detachment of the propylic chain (see Scheme **S5**). Compound at *m/z* 154.0681 (C_8H_9ONF, compound **X**) formation could occur following pathway **E** by thiadiazole ring cleavage; MS^2 analyses and the contemporaneous formation of 5-trifluoromethyl-2-hydroxyl-1,3,4-thiadiazole (**IV**) support the proposed structures (see Scheme **S5**).

Conversely, route **F** involves a defluorination process occurring on the phenyl ring. Compounds at *m/z* 362.0788 (**XI**) has an empirical formula consistent with the substitution of fluorine in the phenyl moiety by an OH group ($C_{14}H_{15}O_3N_3F_3S$). For such, TP **XI** is attributed to 4-

hydroxyl-N-isopropyl-[5-trifluoromethyl)-1,3,4-thiadiazol-2yloxy]acetanilide. Subsequently, N-dealkylation/oxidation on the propylic chain occurs. Compounds at *m/z* 208.0969 (**XII**), 182.0812 (**XIII**), 242.1027 (**XIV**) and 209.1540 (**XV**) all shared an empirical formula consistent with the substitution of fluorine in the phenyl moiety by an OH group and detachment/cleavage of the thiadiazol ring ($C_{11}H_{14}O_3N$, $C_9H_{13}O_3N$, $C_{11}H_{16}O_5N$ and $C_{10}H_{13}O_3N_2S$, respectively) and should all be formed through **XI** transformation (for fragmentation pattern see Scheme **S6**). **XI** transformation could then take place following four main routes accounting for compounds **XII** (see pathway ***F.i*** and scheme **S7**), compound **XIII** (pathway ***F.ii***), **XIV** (pathway ***F.iii***) and **XV** (pathway ***F.iv***) formation. Their transformation further proceeds with the formation of phenol (route ***F.iii*** and ***F.iv***) or catechol (route ***F.i***) and compounds **XVIII** and **XVII** as a result of aminopropylic chain oxidation and dealkylation. TPs at *m/z* 270.0524 (**XX**), 284.0313 (**X**) and 228.0052 (**XXII**) were identified as the major transformation products (see Fig. 5 for time evolution profiles) and are linked together through pathway **G**. All shared an empirical formula well-matched with the detachment of fluorophenyl moiety and involving oxidation or N-dealkylation on the propylic chain. MS^2 analysis allowed to defined the diverse compounds (see Scheme **S8**), all linked together as described in Scheme 3.

3.4. Toxicity evaluation

Acute toxicity was evaluated by monitoring changes in the natural emission of the luminescent bacteria *Vibrio fischeri* when challenged with toxic compounds and is expressed as percentage of inhibition of the bacteria luminescence. Several aqueous samples at different irradiation times were analyzed to estimate the percentage of inhibition of each sample and the data are collected in Fig. 6. The initial toxicity of flufenacet solution showed an inhibition of 32%. Despite the pesticide degradation, after an initial decrease at 5 min of irradiation the toxicity of the solution rapidly increases and reaches a maximum of 66% inhibition at 30 min. After that time, inhibition % slightly

decreases (45 min, inhibition 55%), but remains still higher compared to flufenacet initial toxicity. These observations clearly demonstrate that more toxic transformation products than flufenacet are formed, while synergistic effects among them are also considered. At higher irradiation times the toxicity is smoothly decreased (5% at 120 min of irradiation) until complete detoxification of the irradiated solution is achieved.

3.5. Mineralization process

Even if flufenacet and earlier TPs completely disappears within 60 min of irradiation, the complete mineralization for organic carbon was achieved only after 24 h of irradiation, as shown in Fig. 7. The intermediates described above were degraded themselves, as assessed by Fig. 4 and 5, and after 2h of irradiation they were completely disappeared. At that time, almost 60% of the organic carbon and only 40% of the organic nitrogen were mineralized (see Fig. 7). This proves that derivatives still containing the organic nitrogen are formed. By analyzing the fate of inorganic ions, sulphur atom is stoichiometrically recovered as sulphate ions, while fluoride and nitrogen fate is more intriguing. The nitrogen was partially transformed into ammonium ions (almost 25% of the stoichiometric amount) and nitrite ions, then easily oxidised to nitrate ions (almost 40% of the stoichiometric amount), as shown in Fig. 7. After 24 h only 65 % of the nitrogen is recovered, probably due to a partial photoconversion of N-N into gaseous nitrogen [33]. Fluoride too is only partially recovered (almost 25%). Because fluorine can be easily released from aromatic ring [34], the release of the fluorine atom has to expected from the flufenacet phenyl moiety. Conversely, the lack of fluorine recovery has to be attributed to the $–CF_3$ moiety, whose transformation will reasonably involve the formation of gaseous species, i.e. CHF_3 or CF_3CF_3, not monitored in our experimental conditions.

4. Conclusions

The elimination of flufenacet from water mediated by titania was studied in the present paper. Response Surface Methodology was applied fruitfully for predicting the model and establish the relationships among the variables (TiO_2, H_2O_2 and pH) that affect flufenacet degradation. The results clearly outline the important role of the selection of the most appropriate reaction conditions in achieving highest removal efficiency for specific treatment cases.

The parent compound was easily degraded under treatment and transformed into numerous species. These compounds were identified by means of HRMS and toxicity evaluation showed an increased with their formation. N-Alkylic chain and phenyl moiety were involved into hydroxylation or demethylation reaction, while the thiadiazol moiety is subjected to ring cleavage. Therefore, a tentative reaction pathway was proposed that could match with flufenacet environmental behavior, as already recognised to occur with other environmental pollutants [35-36].

The present study demonstrates the utility and benefits of the experimental design approach for screening and modeling the reaction parameters and. contributes significantly to the improvement and better understanding of photocatalytic process. The latter has shown to be a great potential as a low-cost, environmental friendly and sustainable treatment technology.

References:

[1] O. Ligrini, E. Oliveros, A. Braun, Chem. Rev. 93 (1993) 671-698

[2] M.A. Brown, S.C. DeVito, Crit. Rev. Environ. Sci. Technol. 23 (1993) 249-324.

[3] L. P. Gianessi, M. B. Marcelli, Pesticide Use in U.S. Crop Production, National Summary Report, National Center for Food and Agricultural Policy: Washington, DC, (2000).

[4] European Commission, Health & Consumer Protection Directorate-General, Directorate E – Food Safety: plant health, animal health and welfare, international questions/E1 - Plant health - Flufenacet 7469/VI/98-Final (3 July 2003).

[5] Pest. Management Regulatory Agency, Regulatory Decision Document RDD 2003-07, Flufenacet

[6] US EPA Pesticide Fact Sheet, Flufenacet, Conditional Registration, April 1998, EPA Reg. No. 3125-488.

[7] G. Bischoff, B. Rodemann, W. Pestemer, Entry of Pesticides into surface waters – New results of the Lamspringe run-off monitoring project (1999-2001), XII Symposium Pesticide Chemistry

[8] W.R. Christenson, B.D. Becker, H.D. Hoang, B.S. Wahle, K.D. Moore, P.D. Dass, S.G. Lake, B.P. Stuart, D.L. Van Goethem, G.K. Sangha, J.H. Thyssen, Toxicol. Appl. Pharmacol. 132 (1995) 253-262.

[9] E.A. Guillette, M.M. Meza, M.G. Aquilar, A.D. Soto, I.E. Garcia, Environ. Health Perspect. 106 (1998) 347–353.

[10] D.M. Schreinemachers, Environ. Health Perspect.111 (2003) 1259-1264.

[11] A. Fujishima, K. Hashimoto, T. Watanabe, TiO_2 Photocatalysis, Fundamentals and Applications, Bkc Inc., Tokyo (1999).

[12] I.K. Konstantinou, T.A. Albanis, Appl. Catal. B: Environ. 42 (2003) 319-335

[13] R.F.Teófilo, M.M.C. Ferreira, Quim. Nova 29 (2006) 338-350.

[14] B. de Barros Neto, I.S. Scarminio, R.E. Bruns, in: Planejamento e Otimização de Experimentos, 2a Edição. Unicamp (Ed.), 1996.

[15] G.E.P. Box, W.G. Hunter, J.S. Hunter, in: Statistics for Experiments. An Introduction to Design, Data Analysis and Model Building, Wiley, New York, 1978.

[16] P. Calza, V.A. Sakkas, C. Medana, C. Baiocchi, A. Dimou, E. Pelizzetti, T. Albanis, Appl. Catal. B: Environ. 67 (2006) 197-205

[17] P. Calza, V.A. Sakkas, A. Villioti, C. Massolino, V. Boti, E. Pelizzetti, T. Albanis, Appl. Catal. B: Environ. 84 (2008). 379-388

[18] V.A. Sakkas, P. Calza, C. Medana, A.E. Villioti, C. Baiocchi, E. Pelizzetti, T. Albanis, Appl. Catal. B: Environ. 77 (2007) 135-144

[19] C. Minero, D. Vione, Appl. Catal. B: Environ. 67 (2006) 257-269

[20] C. Minero, Catal. Today 54 (1999) 205-216

[21] A.V. Emeline, V.K. Ryabchuk, N. Serpone, J. Phys. Chem. B 109 (2005) 18515-18521

[22] C.M. So, M.Y. Cheng, J.C. Yu and P.K. Wong, Chemosphere 46 (2002) 905-912

[23] A. Mahalakshmi, B. Arabindoo, A. Palanichamy, V. Murugesan, J. Hazard. Mater. 143 (2007) 240-245

[24] W.Y. Wang and Y. Ku, Colloids Surf. A: Physicochem. Eng. Aspects 302 (2007) 261-268

[25] P. Fernandez-Ibanez, J. Blanco, S. Malato, F.J. de las Nieves, Water Res. 37 (2003) 3180-3188

[26] P. Fernandez-Ibanez, S. Malato, F.J. de las Nieves, Catal. Today 54 (1999) 195-204

[27] J. Wang, W. Sun, Z. Zhang, X. Zhang, R. Li, T. Ma, P. Zhang, Y. Li, J. Mol. Catal. A: Chem. 272 (2007) 84-90

[28] D.F. Ollis Environ. Sci. Technol. 19 (1985) 480–484.

[29] C.S. Turchi, D.F. Ollis, J. Catal. 122 (1990) 192–478.

[30] C.C. Wong, W. Chu, Chemosphere 50 (2003) 981–987.

[31] C.Y. Chan, S. Tao, R. Dawson, P.K. Wong, Environ. Pollut. 131 (2004) 45–54.

[32] L.R. Zimmerman, R. J. Schneider, E. M. Thurman J. Agric. Food Chem. 50 (2002) 1045-1052

[33] P. Calza, E. Pelizzetti, C. Minero, J. Appl. Electrochem., 35 (2005) 665-673

[34] C. Minero, E. Pelizzetti, R. Terzian, N. Serpone, Langmuir 10 (1994) 692-698

[35] P. Calza, S. Marchisio, C. Medana, C. Baiocchi, Anal. Bioanal. Chem. 396 (2010) 1539–1550

[36] P. Calza , C. Medana, E. Raso, V. Giancotti, C. Minero, Sci. Tot. Environ. 409 (2011) 3894-3901

Scheme 1. Fragmentation pathways for species at *m/z* at 380 A -E (compounds from **I-A** to **I-E**)

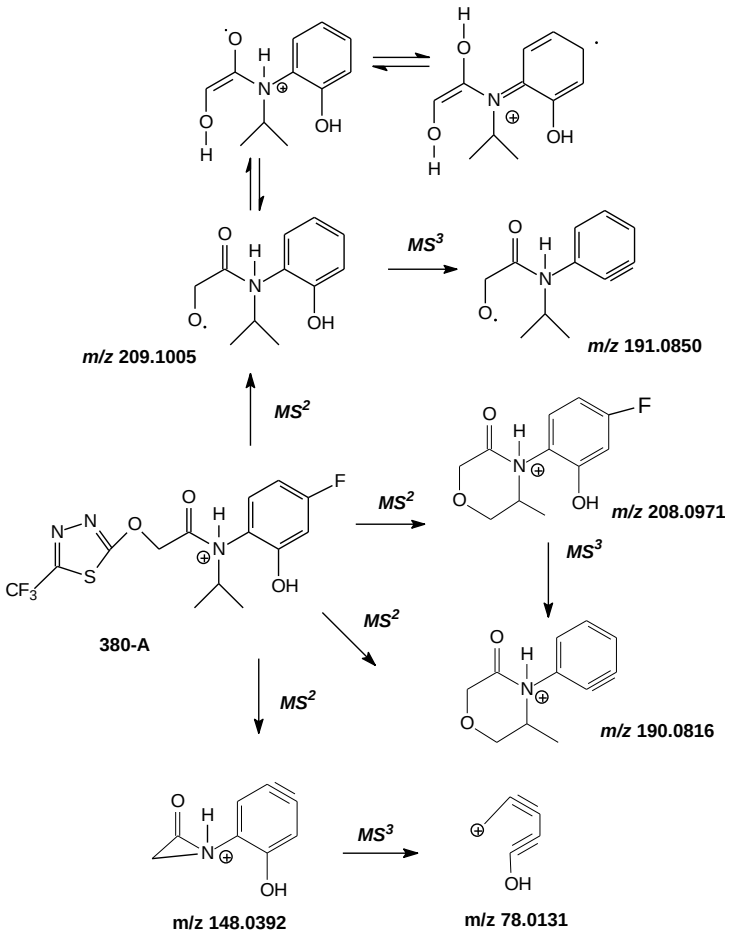

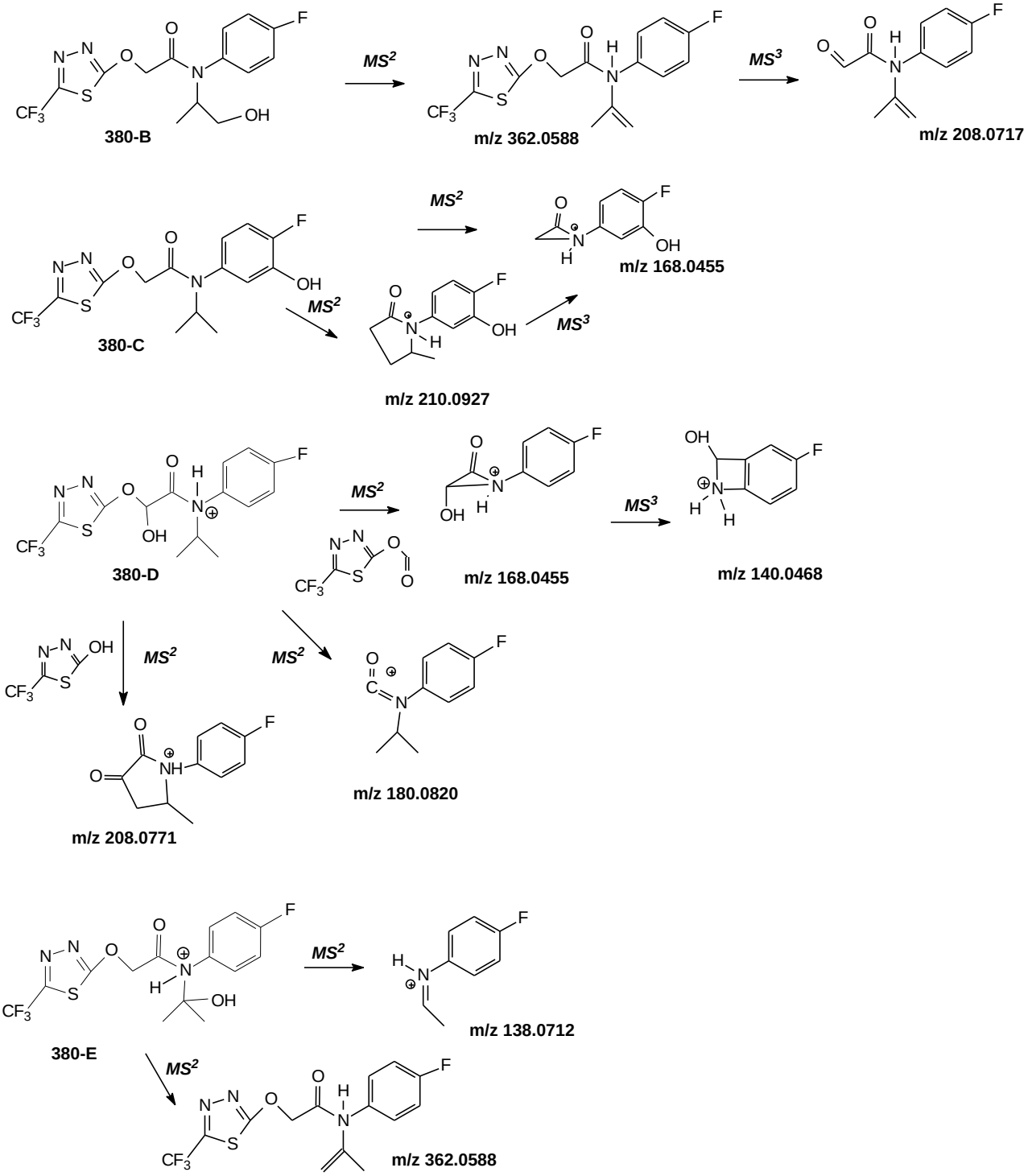
380-B
MS2
m/z 362.0588
MS3
m/z 208.0717
380-C
MS2
m/z 168.0455
MS2
MS3
m/z 210.0927
380-D
MS2
m/z 168.0455
MS3
m/z 140.0468
MS2
MS2
m/z 208.0771
m/z 180.0820
380-E
MS2
m/z 138.0712
MS2
m/z 362.0588

Scheme 2. Proposed flufenacet pathways involving an initial hydroxylation process.

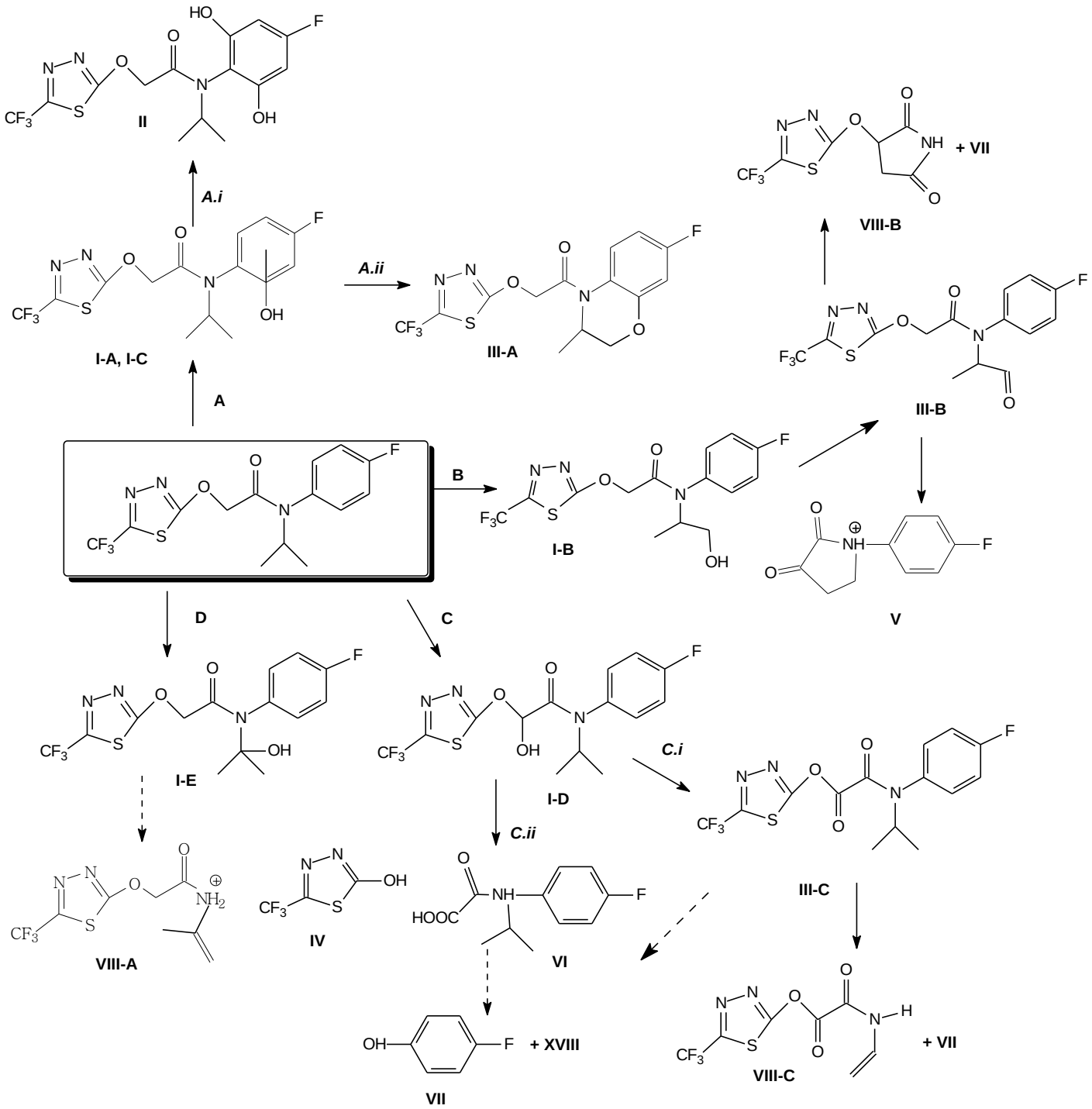

Scheme 3. Proposed flufenacet transformation pathways involving an initial N-dealkylation or defluorination.

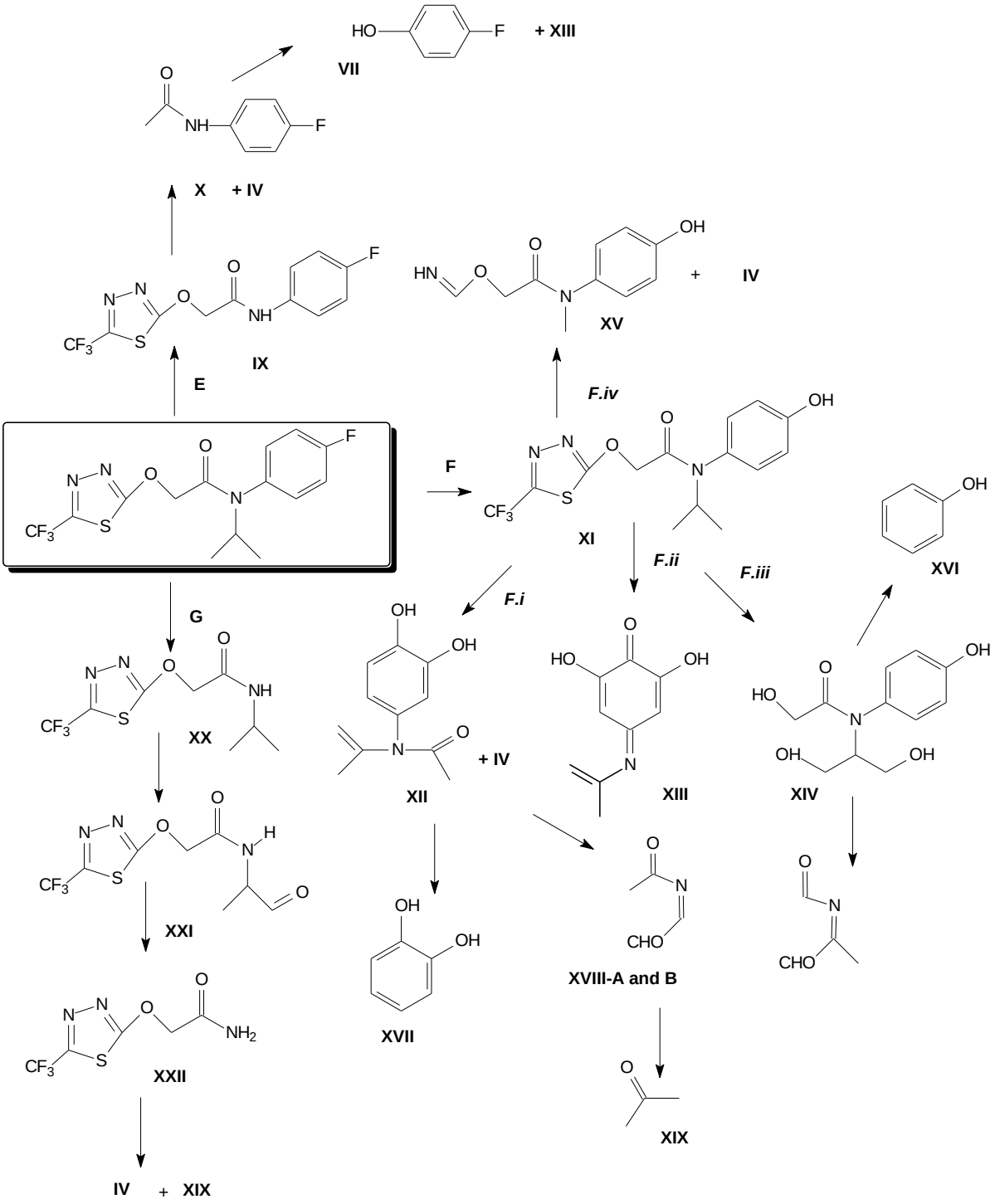

Figure captions

Fig. 1. Pareto Chart of Standardized Effects of the main effects for flufenacet degradation%. The vertical dashed line indicated the level of significance at p=0.05.

Fig. 2. Response surface showing the effect of a) TiO_2 concentration and pH b) H_2O_2 concentration and pH, on the degradation rate expressed as flufenacet degradation% after 30 min irradiation. On axis of TiO_2 value of 0.0 correspond to 500 ppm concentration, on pH axis 0 value correspond to pH 7 and on H_2O_2 axis value 0 correspond to 0.026 M, as described in Table 1.

Fig. 3. Profiles for predicated values and desirability function for flufenacet photocatalytic degradation%. Dashed line indicated current values after optimization.

Fig. 4. Transformation products formed from flufenacet degradation collected in Scheme 2. For all TPs are plotted their area (only 4-Fphenol refers to right y-axis and is plotted in mgL^{-1}) as a function of the irradiation time in the presence of 200 mg/L TiO_2. Panels (a) and (b) collect the more abundant species, while in panel (c) are shown the less abundant species

Fig. 5. Transformation products formed from flufenacet degradation collected in Scheme 3 For all TPs are plotted their area (only phenol and catechol refer to right y-axis and are plotted in mgL^{-1}) as a function of the irradiation time in the presence of 200 mg/L TiO_2. Panels (a) collects the more abundant species, while in panel (b) and (c) are shown the less abundant species.

Fig. 6. Inhibition (%) of the luminescence of bacteria *Vibrio fischeri* as a function of the photocatalytic treatment time in the presence of 200 mg/L TiO_2

Fig. 7. Degradation of flufenacet 15 mg L^{-1} on TiO_2 200 mg L^{-1}; disappearance of the initial compound, TOC profile and evolution of fluoride, sulphate, nitrite, ammonium and nitrate ions.

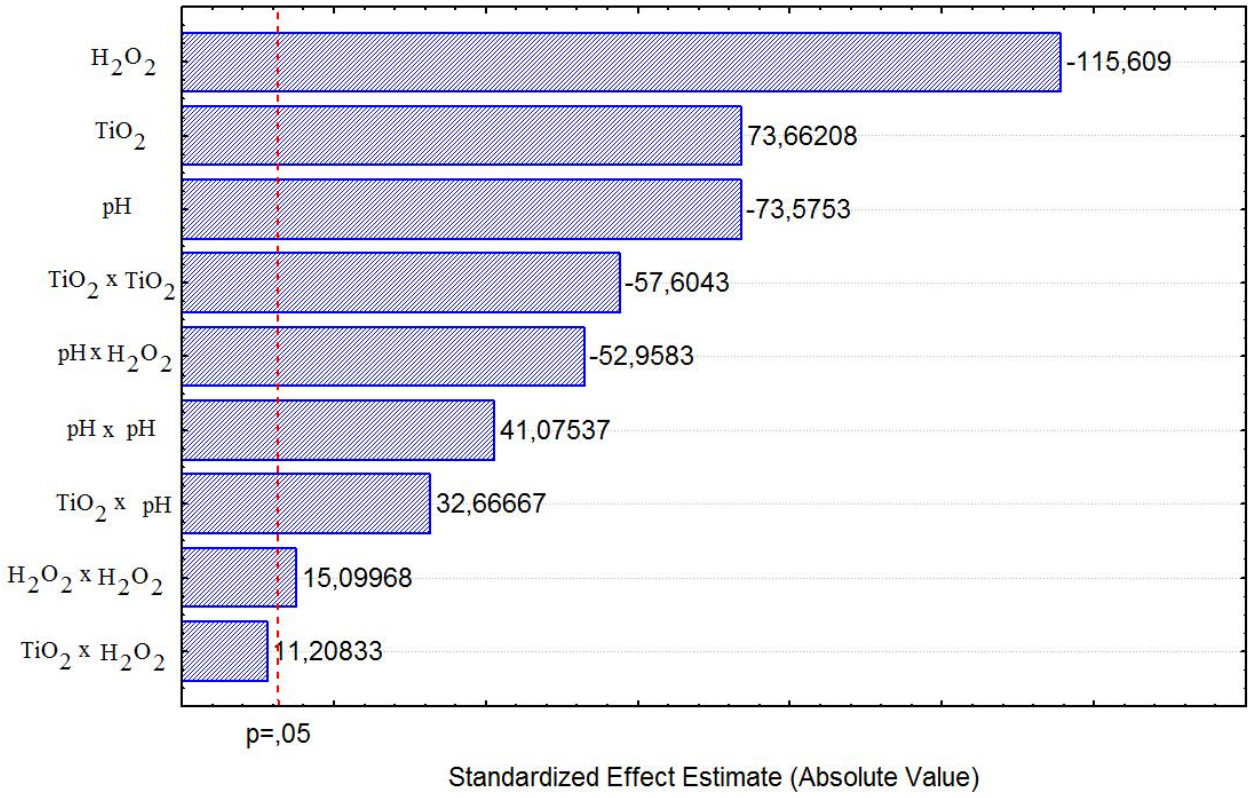
H2O2
TiO2
pH
TiO2 x TiO2
pH x H2O2
pH x pH
TiO2 x pH
H2O2 x H2O2
TiO2 x H2O2
-115,609
73,66208
-73,5753
-57,6043
-52,9583
41,07537
32,66667
15,09968
11,20833
p=,05
Standardized Effect Estimate (Absolute Value)

Fig. 1

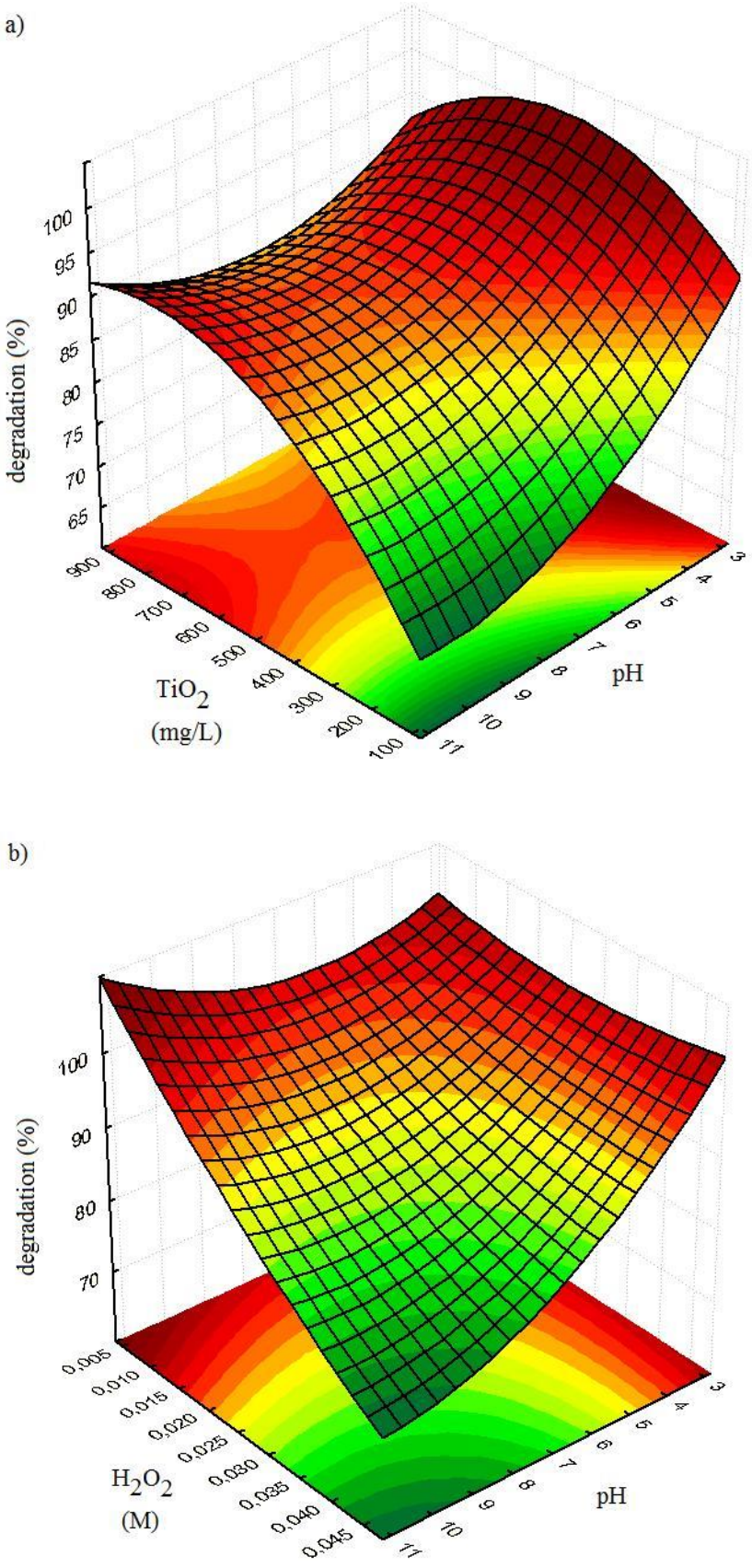
a)
degradation (%)
100
95
90
85
80
75
70
65
900
800
700
600
500
400
300
200
100
TiO2
(mg/L)
3
4
5
6
7
8
9
10
11
pH
b)
degradation (%)
100
90
80
70
0,005
0,010
0,015
0,020
0,025
0,030
0,035
0,040
0,045
H2O2
(M)
3
4
5
6
7
8
9
10
11
pH

Fig.2

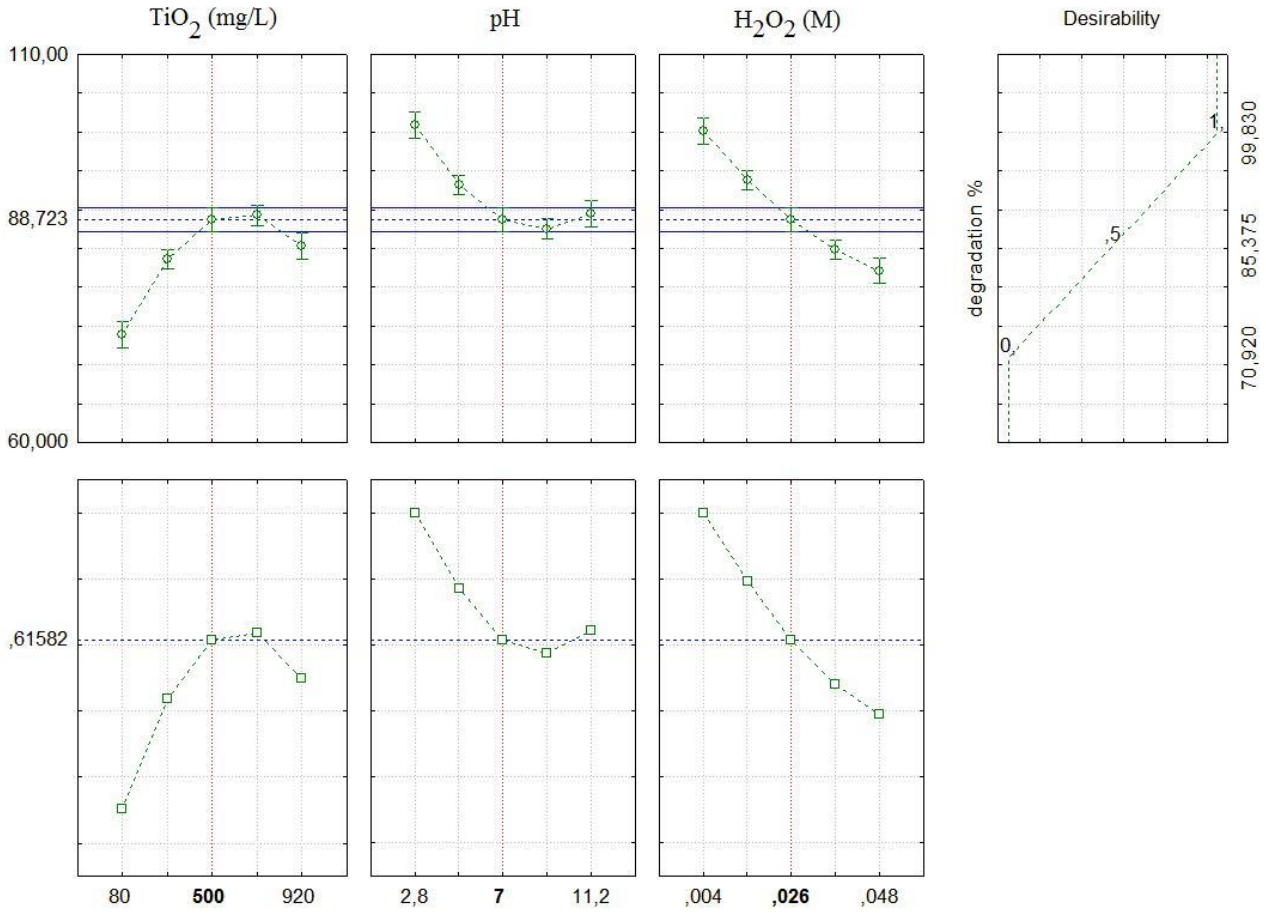
TiO2 (mg/L)
pH
H2O2 (M)
Desirability
110,00
88,723
60,000
,61582
degradation %
99,830
85,375
70,920
1
,5
0
80
500
920
2,8
7
11,2
,004
,026
,048

Fig. 3

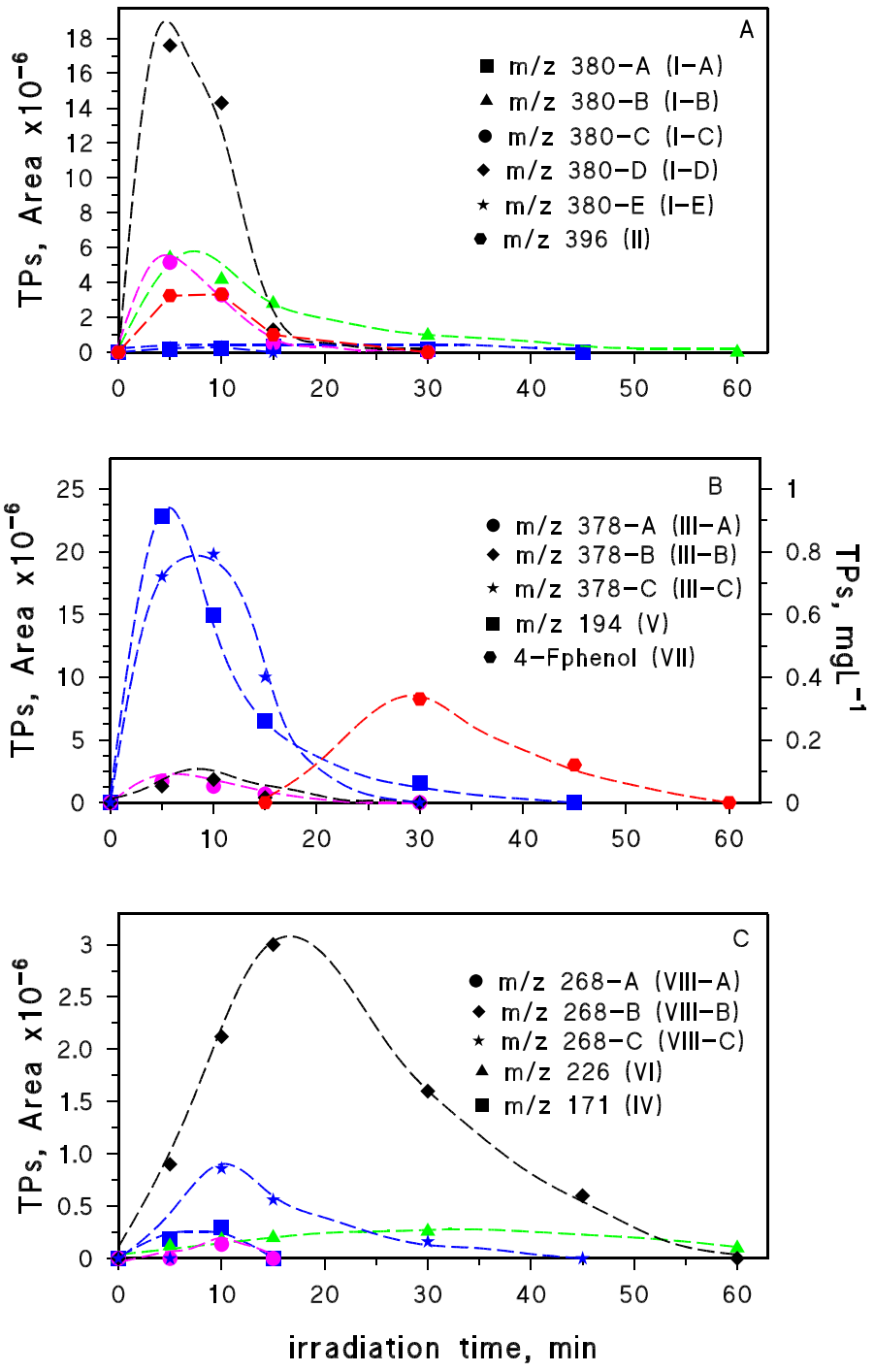
A
m/z 380–A (I–A)
m/z 380–B (I–B)
m/z 380–C (I–C)
m/z 380–D (I–D)
m/z 380–E (I–E)
m/z 396 (II)
TPs, Area x10⁻⁶
B
m/z 378–A (III–A)
m/z 378–B (III–B)
m/z 378–C (III–C)
m/z 194 (V)
4–Fphenol (VII)
TPs, Area x10⁻⁶
TPs, mgL⁻¹
C
m/z 268–A (VIII–A)
m/z 268–B (VIII–B)
m/z 268–C (VIII–C)
m/z 226 (VI)
m/z 171 (IV)
TPs, Area x10⁻⁶
irradiation time, min

Fig. 4

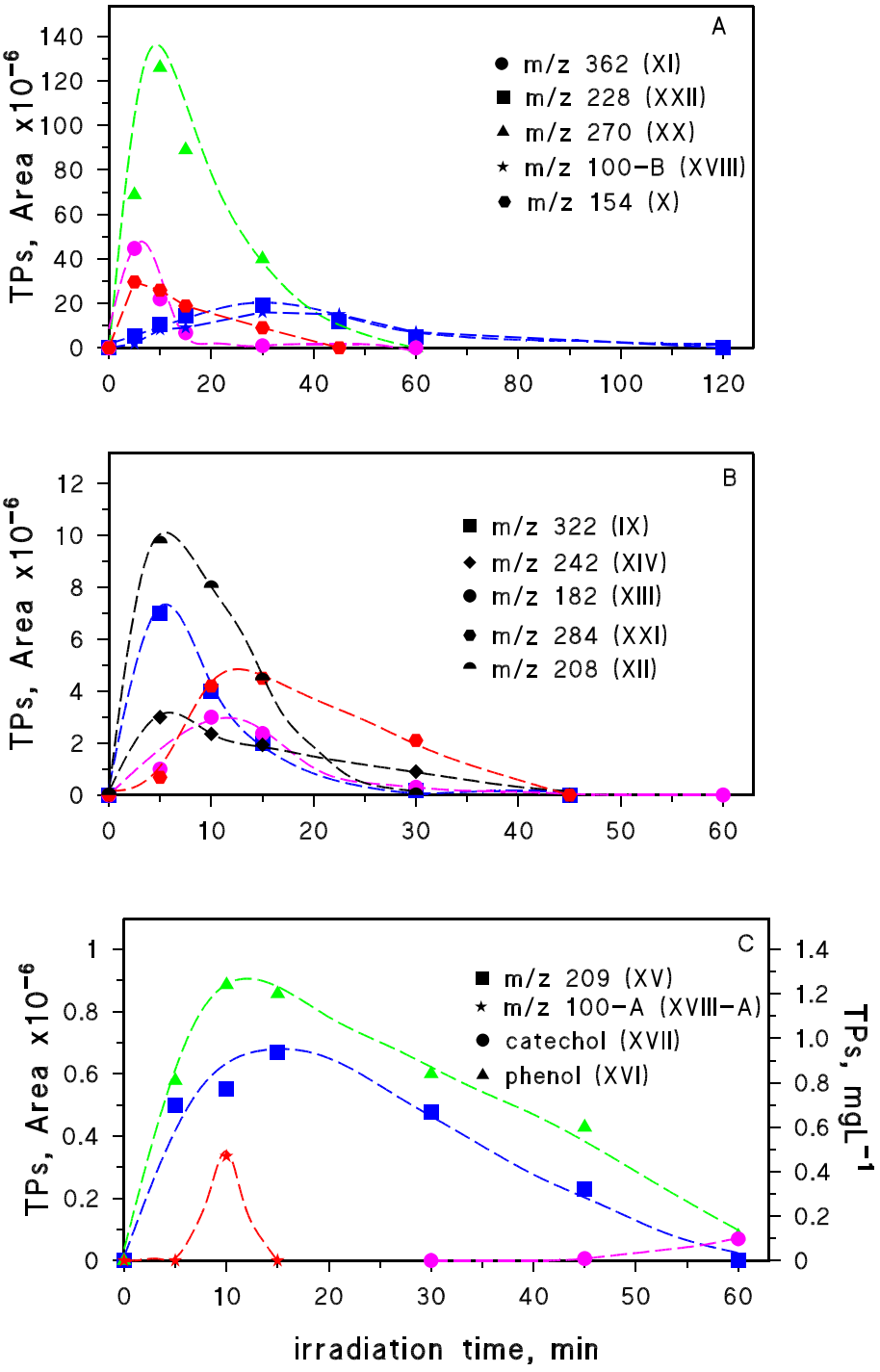
A
m/z 362 (XI)
m/z 228 (XXII)
m/z 270 (XX)
m/z 100-B (XVIII)
m/z 154 (X)
TPs, Area x10⁻⁶
B
m/z 322 (IX)
m/z 242 (XIV)
m/z 182 (XIII)
m/z 284 (XXI)
m/z 208 (XII)
TPs, Area x10⁻⁶
C
m/z 209 (XV)
m/z 100-A (XVIII-A)
catechol (XVII)
phenol (XVI)
TPs, Area x10⁻⁶
TPs, mgL⁻¹
irradiation time, min

Fig. 5

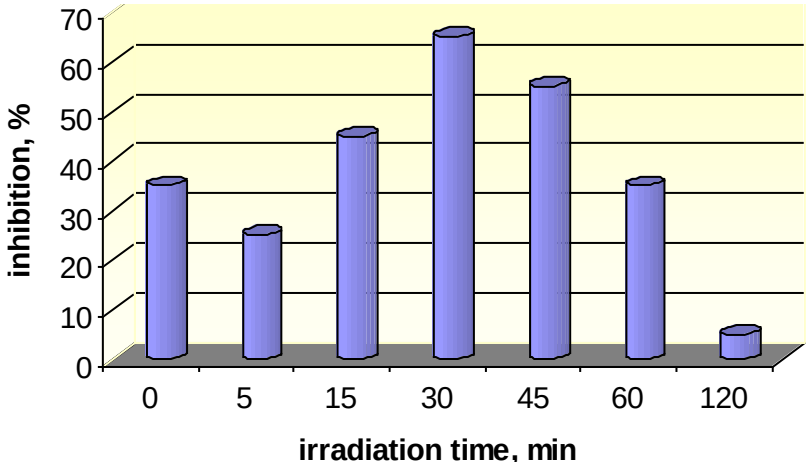
70
60
50
40
30
20
10
0
inhibition, %
0
5
15
30
45
60
120
irradiation time, min

Fig. 6

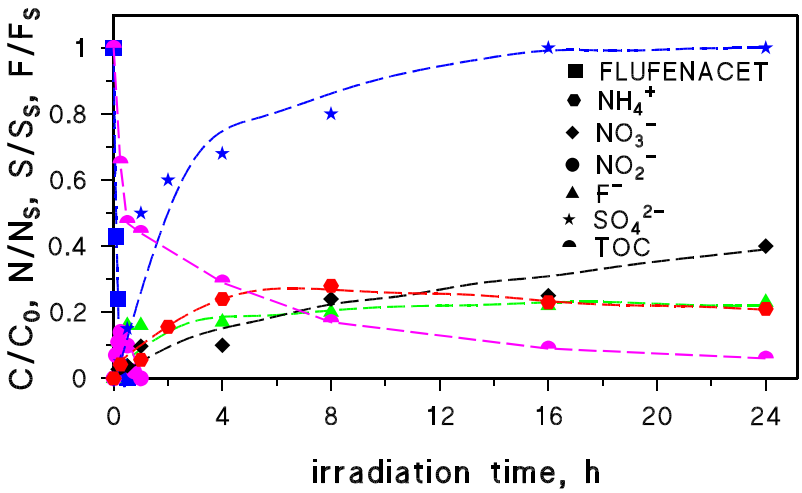
C/C0, N/NS, S/SS, F/FS
1
0.8
0.6
0.4
0.2
0
0
4
8
12
16
20
24
irradiation time, h
FLUFENACET
NH4+
NO3−
NO2−
F−
SO4 2−
TOC

Fig. 7

Table 1. Central composite design matrix for three test variables in coded and natural units along with the observed and the predicted responses

TiO_2 concentration (x_1) mg L^{-1}	pH (x_2)	H_2O_2 concentration (x_3) M	Degradation% (Y observed)	Degradation% (Y predicted)
250 (-1)	4.5 (-1)	0.013 (-1)	94.53	93.39
750 (+1)	4.5 (-1)	0.013 (-1)	95.3	94.89
250 (-1)	9.5 (+1)	0.013 (-1)	90.40	89.07
750 (+1)	9.5 (+1)	0.013 (-1)	97.00	98.41
250 (-1)	4.5 (-1)	0.039 (+1)	90.55	87.78
750 (+1)	4.5 (-1)	0.039 (+1)	92.01	91.97
250 (-1)	9.5 (+1)	0.039 (+1)	71.70	70.75
750 (+1)	9.5 (+1)	0.039 (+1)	83.03	82.78
500 (0)	7.0 (0)	0.026 (0)	88.76	88.93
500 (0)	7.0 (0)	0.026 (0)	88.99	88.93
80 (-1.68)	7.0 (0)	0.026 (0)	70.92	73.94
920 (+1.68)	7.0 (0)	0.026 (0)	86.43	85.31
500 (0)	2.8 (-1.68)	0.026 (0)	98.96	100.88
500 (0)	11.2 (+1.68)	0.026 (0)	89.53	89.52
500 (0)	7.0 (0)	0.004 (-1.68)	99.83	100.04
500 (0)	7.0 (0)	0.048 (+1.68)	80.50	82.20

Table 2. Main $[M+H]^+$ and fragments coming from MS and MS^n spectra obtained from flufenacet and its intermediate compounds collected in Scheme 2.

$[M+H]^+$ and empirical formula	**Δmmu**	**t_R**	**MS^2**	**MS^3 [MS^4]**
FLUFENACET 364.0774 $C_{14}H_{14}F_4N_3O_2S$	3.663	24.83	**194.0964** (100) $C_{11}H_{13}ONF$	**152.0494 (**70) C_8H_7ONF
				124.0545(100) C_7H_7NF
				97.0436 (5) C_6H_6F
			152.0494 (50) C_8H_7ONF	**124.0545**(100) C_7H_7NF
			124.0545(10) C_7H_7NF	**97.0436**(100) C_6H_6F
(I-A) 380-A (380,0692) $C_{14}H_{14}O_3N_3F_4S$	0.549	18.22	**208.0918** (75) $C_{11}H_{11}O_2NF$	**190.0816** (100) $C_{11}H_{12}O_2N$ [**MS^4**: **148.0392** (100)$C_8H_6O_2N$]
			209.1005 (100) $C_{11}H_{15}O_3N$	**191.0850** (100) $C_{11}H_{13}O_2N$ [**MS^4**: **149.0389** (100) $C_8H_7O_2N$]
			210.0971 (5) $C_{11}H_{13}O_2NF$	**191.0850 (**100) $C_{11}H_{13}O_2N$
			191.0850 (50) $C_{11}H_{12}O_2N$	**149.0389** (100) $C_8H_7O_2N$
			190.0816 (30) $C_{11}H_{12}O_2N$	**148.0392** (100) $C_8H_6O_2N$
			148.0392 (10) $C_8H_6O_2N$	**120.5745**(50)
				78.0131 (40)
(I-B) 380-B	0.549	19.94	**362.0588** (100) $C_{14}H_{12}O_2N_3F_4S$	**208.0918** (100) $C_{11}H_{11}O_2NF$ [**MS^4**:**152,0869** (100)$C_9H_{11}NF$]
(I-C) 380-C	0.549	21.33	**210.0927** (100) $C_{11}H_{13}O_2NF$	**168.0455** (100) $C_8H_7O_2NF$
			168.0455 (20) $C_8H_7O_2NF$	**-**
(I-D) 380-D	0.549	22.84	**168.0455** (100) $C_8H_7O_2NF$	**140.0468** (100) C_7H_7ONF
			208.0771 (75) $C_{11}H_{11}O_2NF$	**-**
			209.0804 (70)	
			180.0775 (20) $C_{10}H_{11}ONF$	**-**
			181.0850 (30)	
(I-E) 380-E	0.549	25.38	**362.0588** (100) $C_{14}H_{12}O_2N_3F_4S$	-
			138.0712 (40) C_8H_9NF	-
(II)- 396.0634 $C_{14}H_{14}O_4N_3F_4S$	-0.160	18.64	**184.0358** (100) $C_8H_7O_3NF$	**142.0261** (65) $C_6H_5O_2NF$
			226.0878 (30) $C_{11}H_{13}0_3NF$	**184.0358** (65) $C_8H_7O_3NF$
			141.0345 (20) $C_7H_6O_2F$	-
(III-A) 378-A 378.0536 $C_{14}H_{12}O_3N_3F_4S$	0.559	18.10	**208.0918** (100) $C_{11}H_{11}O_2NF$	**190.0816** (100) $C_{11}H_9ONF$
				148.0354 (25) $C_8H_5O_2NF$
			190.0816 (50) $C_{11}H_9ONF$	**148.0354** (100) $C_8H_5O_2NF$
			148.0354 (20) $C_8H_5O_2NF$	**-**
(III-B) 378-B	0.559	20.48	**208.0918** (100) $C_{11}H_{11}O_2NF$	**180.0775** (70) $C_{10}H_{11}ONF$
			180.0775 (50) $C_{10}H_{11}ONF$	-
(III-C) 378-C	0.559	22.95	**208.0918** (100) $C_{11}H_{11}O_2NF$	**180.0775** (100) $C_{10}H_{11}ONF$
			180.0775 (50) $C_{10}H_{11}ONF$	**136.0521** (100) C_8H_7NF
				150.0674 (90) C_9H_9NF
				152.0868 (90) $C_9H_{11}NF$
			150.0674 (20) C_9H_9NF	-
(IV) 170.9810 $C_3H_2N_2F_3S$	-2.445	13.18	-	-
(V) 194.0613	0.157	23.27	**136.0521** (100) C_8H_7NF	**-**

$C_{10}H_9O_2NF$				
(VI) 226.0899 $C_{11}H_{13}O_3NF$	2.502	1.1	-	-
(VIII) 268-A 268.0372 $C_8H_9O_2N_3F_3S$	0.410	6.40	**114.0546** (100) $C_5H_8O_2N$	**58.0643** (100) C_3H_8N
(VIII-B) 268-B 268.0102 $C_7H_5O_3N_3F_3S$	0.410	12.0	**114.0192** (100) $C_4H_4O_3N$	**58.0293** (100) C_3H_8N
(VIII-C) 268-C 268.0102 $C_7H_5O_3N_3F_3S$	0.410	14.48	**-**	-

Table 3. Main $[M+H]^+$ and fragments coming from MS and MS^n spectra obtained from flufenacet intermediate compounds collected in Scheme 3.

$[M+H]^+$	**Δmmu**	**t_R**	**MS^2**	**MS^3**
(IX) 322.0273 $C_{11}H_8O_2N_3F_4S$	0.713	21.44	**152.0494** (60) C_8H_7ONF	-
			124.0545 (100) C_7H_7NF	**-**
			109.0443 (25) C_7H_6F	**-**
(X) 154.0661 C_8H_9ONF	0.313	12.40	**112.0553** (100) C_6H_7NF	-
(XI) 362.0788 $C_{14}H_{15}O_3N_3F_3S$	0.727	20.26	**208.0770** (100) $C_{11}H_{14}O_3N$	-
(XII) 208.0969 $C_{11}H_{14}O_3N$	0.070	18.32	**190.0863** (100)$C_{11}H_{12}O_2N$	**148.0392** (100) $C_8H_6O_2N$
(XIII) 182.0812 $C_9H_{13}O_3N$	0.010	18.54	**140.0340** (100) $C_6H_6O_3N$	-
(XIV) 242.1027 $C_{11}H_{16}O_5N$	0.413	14.77	**182.0811** (100) $C_9H_{12}O_3N$	-
			154.0861 (100) $C_8H_{12}O_2N$	-
(XV) 209.1540	0.317	20.58	-	-
(XVIII-A) 100.0389-A $C_4H_6O_2N$	-0.445	14.24	-	-
(XVIII-B) 100.0389-B $C_4H_6O_2N$	-0.445	15.22	**-**	-
(XX) 270.0524 $C_8H_{11}O_2N_3F_3S$	0.512	16.60	**100.0752** (100) $C_5H_{10}ON$	**72.0801** (100) $C_4H_{10}N$
				58.0644 (20) C_3H_8N
			72.0801 (50) $C_4H_{10}N$	-
(XXI) 284.0313 $C_8H_9O_3N_3F_3S$	0.217	11.33	**114.0546** (100) $C_5H_8O_2N$	**86.0595 (**65) C_4H_8ON
				58.0644 (100) C_3H_8N
(XXII) 228.0052 $C_5H_5O_2N_3F_3S$	0.280	11.01	**210.9786** (100) $C_5H_2O_2N_2F_3S$	**123.0161** (100) $C_3H_2N_2F_3$
				96.0051 (50) C_2HNF_3